

# Wind Turbine Maximum Power Point Tracking Using Integrated Generator–Rectifier Systems

G. Sandeep S.Prakash

GOKULA KRISHNA COLLEGE OF ENGINEERING

Submitted: 01-12-2021

Revised: 11-12-2021

Accepted: 14-12-2021

**ABSTRACT-** Offshore wind is a fast-expanding source of renewable energy. To obtain a competitive levelized cost of electricity, offshore energy harvesting requires multimegawatt wind turbines and high efficiency, high power density, and reliable power conversion equipment. An electromechanical power conversion system that combines one active and numerous passive rectifiers with a multiport permanent magnet synchronous generator is a viable option. Maximum power point tracking (MPPT) capability is required for the deployment of integrated systems in offshore wind energy, which is difficult due to the existence of several uncontrolled passive rectifiers. The viability of MPPT is demonstrated in this article based on the discovery that the active-rectifier d-axis current can control the overall system output power. The MPPT capability expands the range of applications for integrated systems in offshore wind.

**Index Terms**—AC–DC power conversion, dc power systems, maximum power point trackers (MPPT), power conversion, rectifiers, wind energy, wind energy generation.

## 1. INTRODUCTION

Offshore wind is a rapidly growing renewable energy resource [2–5]. Offshore wind turbines with outputs that exceed the usual land-based power output have recently been developed in order to achieve a competitive levelized cost of electricity (LCOE). Gamesa 10X [6], Haliade X [7], and Vestas V164 [8], for example, have power ratings of 10 to 12 MW. It is difficult to develop high-power-density, efficient, and reliable electromechanical power conversion systems for these turbines using traditional converter topologies. Limited power-electronics-switch voltage/current ratings and excessive switching losses are the key roadblocks [9]. The most prevalent architectures are two-level pulse width

modulation (PWM) and neutral-point-clamped converters.

The former has a clear control scheme and a simple construction [10]–[12]. The peak ac-side current and dc-side voltage are rated for each switch. To process the multimegawatt power, available power electronics devices are coupled in series and/or parallel. The reliability of these combinations is poor [13]. The neutral-point-clamped layout minimises each switch's voltage rating needs [14]–[16]. The loss distribution throughout the switches is uneven, resulting in early failure at the hot spots. Multiport generators [17]– [19] have been presented as a way to lower the power rating of individual power converters. For ac to dc conversion, all of these systems rely only on an active rectifier.

A combined generator–rectifier system based on a permanent magnet synchronous generator (PMSG), as shown in Fig. 1(a), is a viable option [20], [21]. A multiport PMSG converts the mechanical power on the turbine shaft to ac electrical power. For ac–dc conversion, each port is linked to either a passive or active rectifier. The rectifiers' dc outputs are connected in series to form a reasonably high-voltage dc bus. Only a part of the total dc-bus voltage is supported by each rectifier. As a result, passive rectifiers process 60% of total power, resulting in a 47 percent reduction in conversion loss at the rated working state. Because the active-rectifier size is reduced, the overall system power density and reliability improve.

Due to the existence of several passive rectifiers, power-flow regulation in the combined generator–rectifier system is difficult. The main contribution of this paper is to show that even with a sequence of uncontrolled passive rectifiers, a controllable total dc-bus power flow may be accomplished. Maximum power point tracking (MPPT), which is critical in wind-energy

applications [10], [22]–[24], is enabled by the ability to manage the power flow. To achieve MPPT, a control framework based on a relationship between the active-rectifier d-axis current and the total dc-bus power is proposed. Filter capacitors are also removed from the passive-rectifier outputs. By adjusting the corresponding phases of different ac ports supplying the passive rectifiers, the dc-bus voltage ripple is reduced. The integrated generator–rectifier system promises to lower the offshore-

wind LCOE thanks to MPPT management and the removal of bulky filter capacitors.

The remainder of this article is structured in the following manner. The power-flow control framework for the integrated generator–rectifier system is discussed in Section II, and this methodology is applied to MPPT. Sections III and IV, respectively, give simulation and experimental evidence to support the findings. Finally, Section V brings this article to a close.

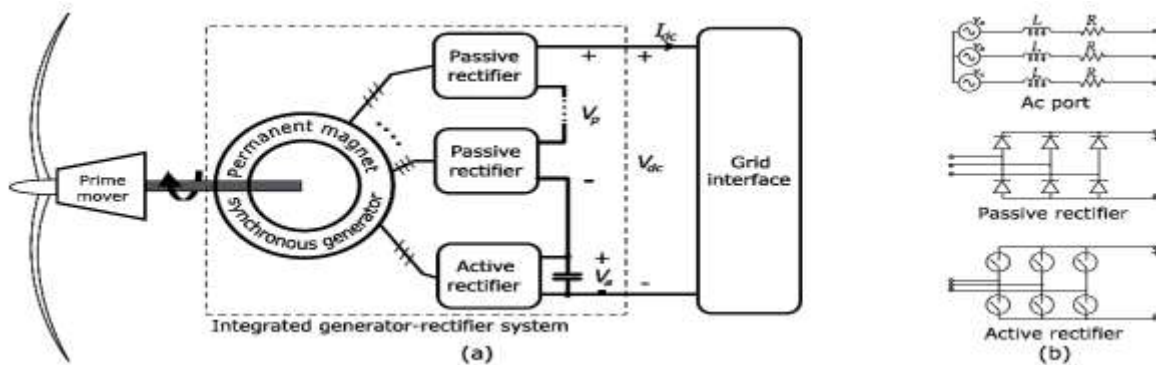


Fig. 1. (a) Wind turbine power-point tracking architecture: the prime mover is a variable-speed wind turbine. The turbine shares a common shaft with the multiport PMSG. AC power is converted to dc by an integrated generator–rectifier system. The dc output is connected to a stiff dc interface. The integrated generator–rectifier

system performs maximum power-point tracking to extract the turbine maximum power. (b) Each phase of a three-phase ac port is modelled by a back EMF source in series with generator inductance  $L$  and phase resistance  $R$ . The passive rectifier is a six-pulse diode rectifier, and the active rectifier is a three-phase two-level converter.

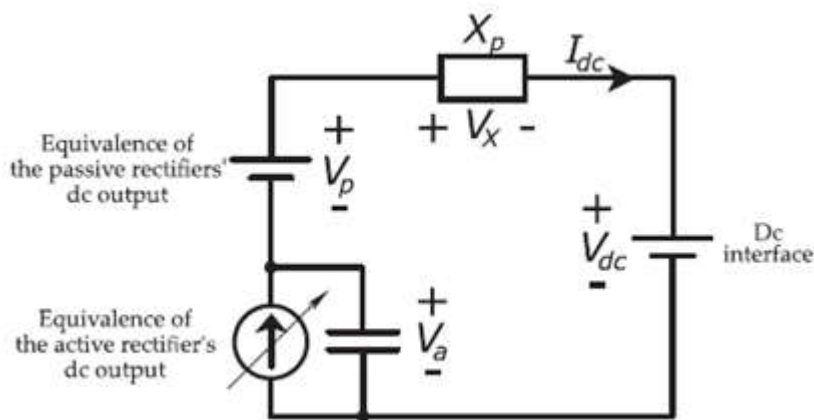


Fig. 2. Simplified equivalent circuit of the integrated generator–rectifier system.

The dc output of the passive rectifiers is modeled by a voltage source. The output of the active rectifier is modeled by a controllable current source. The serial voltage and current sources are connected to a constant dc voltage representing the dc interface.

## II. INTEGRATED GENERATOR–RECTIFIER SYSTEM POWER-FLOW CONTROL

The power-flow control framework for the proposed combined generator–rectifier system is developed in this section. It is assumed that the

system's dc output is coupled to a stiff dc interface. For both ac and dc collection grids, this assumption is true [9]. In the case of ac, the interface is a grid-side converter-controlled intermediate dc bus. The dc voltage is controlled by a converter at the dc-grid substation in the dc case [25], [26].

Figure 2 depicts a simplified equivalent circuit of the integrated system. The total output of the passive rectifiers is represented by  $V_p$ , a generator-speed-dependent voltage source in series with  $X_p$ , a commutation reactance. The voltage ripple of the overall passive-rectifier output can be ignored by establishing a phase shift among distinct ac ports, as stated in Section II-A. The difference between the continuous grid interface voltage,  $V_{dc}$ , and the passive-rectifier output voltage determines the active-rectifier dc-side voltage,  $V_a$ .

The active rectifier's dc-side current is determined by the adjustable power it draws. A controlled current source is used to represent the active rectifier. The quantity of power flowing into the dc bus is determined by the current flowing out of the active rectifier, as explained in Section II-B. For practical implementation, cascaded proportional-integral (PI) controllers are presented. In Section II-C, the power-flow control framework is used to accomplish MPPT.

### A. Voltage-Ripple Minimization in Passive Rectifiers

In the case of a PMSG with  $k$  three-phase ac ports, the  $(k - 1)$  ports power passive rectifiers without output filter capacitors. As illustrated in Fig. 3(a), each passive rectifier's dc-output voltage ripple has a peak every  $\frac{\pi}{3}$  radians. The voltage ripple percentage, defined as the ratio between the peak-to-peak ripple and the average value, is minimized when the dc outputs are connected serially with an adequate phase shift. As demonstrated in Fig. 3(b), the ripple percentage of two passive rectifiers with  $\frac{\pi}{6}$  phase shifting is 3%, against 14% without phase shifting.

Fig. 3(b). shows that without phase shifting, only 14% of the population is affected. In general, a  $3(k-1)$  radian phase shift reduces voltage ripple in a system with  $(k-1)$  passive rectifiers. As demonstrated in Fig. 3(c), increasing the number of ac ports reduces the voltage ripple percentage, although at a decreasing pace. This method is analogous to the employment of multipulse diode rectifiers and phaseshifting transformers to reduce linecurrent harmonic distortion in high-power drives [27]. The total dc output voltage of  $(k-1)$  passive rectifiers at the electrical frequency is  $\omega$ , assuming no voltage ripple and a constant dc-bus current  $I_{dc}$ .

$$V_{\text{passive}} = \frac{3}{\pi} (k - 1) \sqrt{3E(\omega)} - (k - 1) \left( \frac{3}{\pi} \omega L + 2R \right) I_{dc} \quad (1)$$

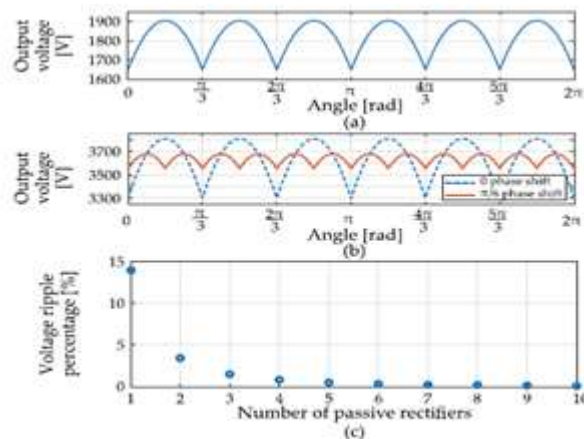


Figure 3 shows example output voltage waveforms from the integrated system in Figure 1, with each ac port generating 1.1 kV peak line-to-neutral voltage at a frequency of 20 Hz. (a) One passive rectifier's DC output voltage. (b) DC output voltage of two passive rectifiers connected in series with/without phase shifting between the corresponding ac ports, with or without phase shifting. (c) As the number of passive ports grows,

the ratio between the voltage  $V_p$  peak-to-peak ripple and the average value decreases. where  $L$  and  $R$  are the per-phase equivalent series resistance and synchronous inductance of each ac port, respectively [28]. Electrical frequency affects the back EMF  $E(\omega)$ .

$$E(\omega) = \frac{\omega}{2\pi f_0} E_0 \quad (2)$$

Each ac port's rated electrical frequency and rated line-to-neutral peak back EMF are denoted by  $f_0$  and  $E_0$ , respectively. The effects of the synchronous inductance, phase resistance, and dc-bus current on the dc-side voltage of the passive rectifier are captured by the word  $V_X$ . The synchronous inductance is considered to be low enough that phase current commutation takes less than one-sixth of the electrical period, which corresponds to Mode I operation of a six-pulse diode bridge rectifier [28].

### B. Active Rectifier to Control Power Flow

$$V_a = V_{dc} - V_p + X_p I_{dc} \quad (4)$$

The dc-bus current is represented by

$$I_{dc} = P_{dc} / V_{dc} \quad (5)$$

where  $P_{dc}$  is the dc-bus power. Substituting (4) and (5) in (3), the dc-bus power relates to the active-rectifier d-axis current by

$$\frac{3}{2} E(\omega) I_{sd} - \frac{3}{2} I^2_{sd} R = P_{2dc} \left( (k - 1) \frac{1}{\sqrt{2} V_{dc}} \left( \frac{3}{\pi} \omega L + 2R \right) + P_{dc} \left( 1 - \frac{3}{\pi} (k - 1) \frac{\sqrt{3} E(\omega)}{V_{dc}} \right) \right) \quad (6)$$

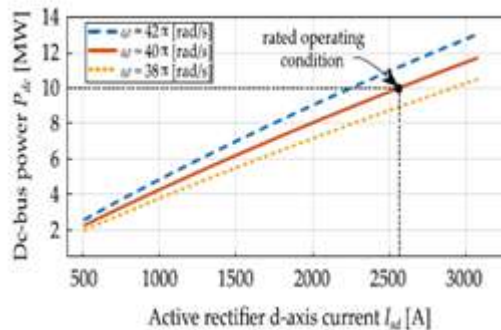


Fig. 4. At each generator speed, the power drawn from the integrated generator-rectifier system depends on the active-rectifier d-axis current resistance of 12 m, and a synchronous inductance  $L$  of 0.47 mH. At the rated operating state, these values correspond to 0.02 p.u. resistance and 0.1 p.u. synchronous reactance, respectively. The relationship is also shown at two different electrical frequencies to show how power control can be used to regulate generator speed.

A cascaded architecture, as shown in Figure 5, is used to control power flow. The active

$$L \frac{dI_{sd}}{dt} = -R I_{sd} + \omega L I_{sq} + E - V_{rd} \quad \text{and} \quad (7)$$

$$L \frac{dI_{sq}}{dt} = -R I_{sq} - \omega L I_{sd} - V_{rq} \quad (8)$$

The next step is to calculate the ac-side current of the active rectifier and the dc-bus power. The power balance between the ac and dc sides leads to  $t$  when conversion losses in the active rectifier are ignored.

$$\frac{3}{2} E(\omega) I_{sd} - \frac{3}{2} I^2_{sd} R = V_a I_{dc} \quad (3)$$

where  $V_a$  is the active-rectifier dc-side voltage and  $I_{sd}$  is the active-rectifier ac-side current's d-axis component. The peak phase-A back EMF is aligned with the d-axis. Using Fig. 2 as a guide

The active-rectifier d-axis current can control the power flowing into the dc-bus, or, equivalently, the power pulled from the turbine, as shown in Equation (6). Using a 10MW wind-turbine system with a three-port PMSG, Fig. 4 depicts the link between  $I_{sd}$  and  $P_{dc}$ . Each port has a back EMF of 1.1kV at a frequency of 20Hz, an equivalent series

rectifier's d-axis and q-axis currents are regulated by current controllers in the inner loop. The power flow and power factor are controlled by the d-axis and q-axis currents, respectively. The d-axis current command is calculated by the outer-loop power controller to send the reference power  $P_{dc}$  to the dc bus. An MPPT algorithm that employs generator rotational speed as an input produces the power command. When the q-axis current is set to zero, the active rectifier operates at unity power factor. The current controllers are built using the ac-port current dynamics in the dq reference frame.

The input d-axis and q-axis voltages are  $V_{rd}$  and  $V_{rq}$ , respectively. The peak phase-A back EMF is aligned with the d-axis. The q-axis is 90 degrees ahead of the d-axis. To generate the d-axis voltage command,

controller with feed-forward terms is chosen using (7).

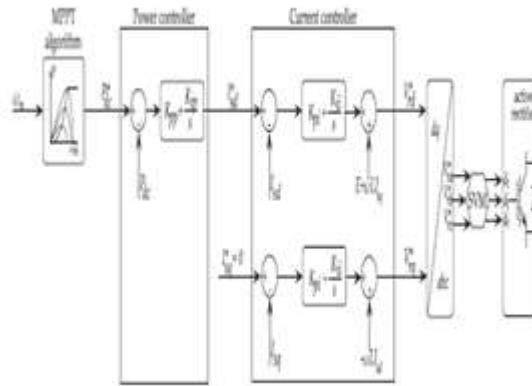


Fig. 5. Cascaded architecture applied to the active rectifier to accomplish power-flow control for the entire integrated generator–rectifier system.

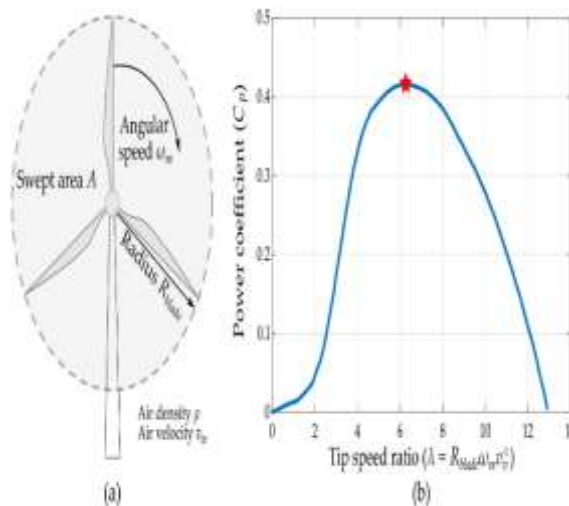


Fig. 6. (a) Illustration of a three-bladed wind turbine. (b) Typical wind-turbine power coefficient versus tip-speed ratio curve [29].

$$V^*rd = Kpi(I^*sd - Isd) + [Kii(I^*sd - Isd)dt + E + \omega 0LIsq] \quad (9)$$

The reference d-axis current, proportional, and integral gains, respectively, are  $I^*sd$ ,  $Kip$ , and  $Kii$ . The q-axis current controller can be created similarly using (8). With precise prior knowledge of  $L$  and  $R$ , the d-axis current command for a specified power requirement can be calculated directly (6). Using an outer-loop PI control, given by, the impact of any parametric uncertainties on the power flow control can be minimised.

$$I^*sd = Kpp(P^*dc - Pdc) + Kip \int (P^*dc - Pdc)dt \quad (10)$$

where  $Kpp$  and  $Kip$  are the proportional and integral gains, respectively.

### C. MPPT Using Integrated Generator–Rectifier System

The proposed power-control architecture is used to track the maximum power point of a wind turbine. MPPT is obtained if the electrical power drawn at each generator speed follows the maximum power curve [23]. Consider the wind turbine in Fig. 6 with  $R_{blade} = 164$  m, working at 12 m/s rated wind speed and 1.15 kg/m<sup>3</sup> air density. The mechanical power curves of the wind

turbine are plotted in Fig. 7 using dashed lines at various wind speeds. The peak values of all the

mechanical power curves are connected to generate the maximum power curve.

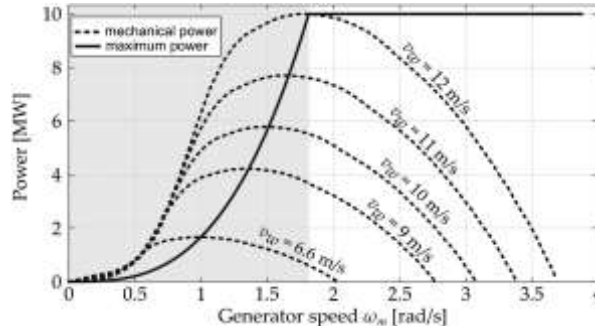


Fig. 7. Mechanical power curves and maximum power curve of a 10 MW wind turbine.

Assume a wind speed of 12 m/s for the procedure. The graph is divided into two parts by a vertical line that crosses the intersection of the maximum power curve and the mechanical power curve. The input mechanical power to the generator is greater than the output electrical power in the grey zone. The rotating speed of the generator

increases. The generator then moves into the white area, where mechanical power is less than electrical power. The generator begins to slow down. The speed eventually settles at the border between the two sectors, where the maximum power of 10 MW is created.

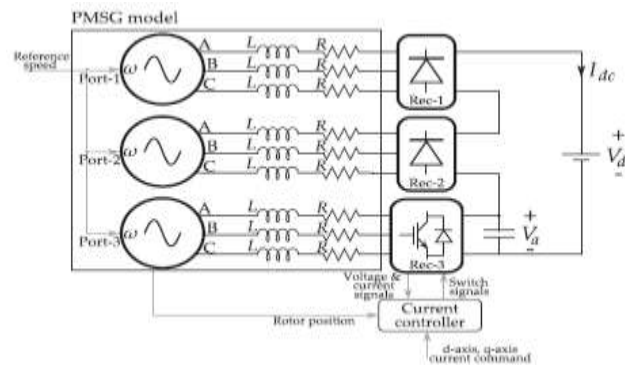


Fig. 8. Simulation model based on a three-port PMSG with integrated power electronics used to illustrate the drive-train operation at different generator speeds

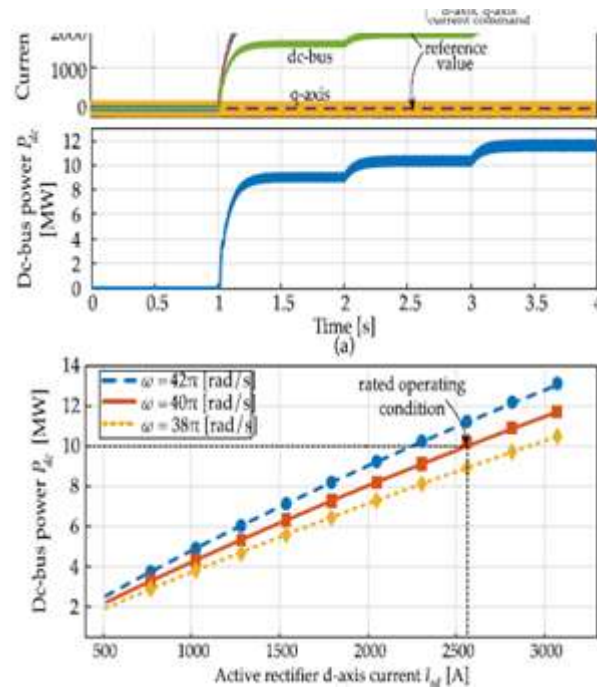


Fig. 9. (a) (Top plot) Active-rectifier d-axis and q-axis currents track the reference command, presented by the dotted lines. The dc-bus current varies accordingly by changing the d-axis current, leading to a change in the dc-bus power (bottom plot). (b) Relationship between dc-bus power and active-rectifier d-axis current acquired from the simulation model (recorded by the markers) matches the theoretical analysis [plotted by the lines using (6)].

The active-rectifier d-axis current is shown as the dc-bus power control input in Fig. 9(a). When the q-axis current is instructed to remain at zero, the upper plot depicts current waveforms corresponding to various active-rectifier d-axis current reference values. The current in the dc-bus is equal to the current in the d-axis.

According to the bottom plot of Fig. 9(b), dc-bus power varies proportionally to dc-bus current Fig. 9(b) shows the verification of the theoretical analysis, (6). At generator speeds of 38, 40, and 42 rad/s, different dc-bus power levels are measured, whereas the d-axis current ranges from 500 to 3100 A. The diamond, square, and circle markers are used to illustrate the recorded dc-bus

power versus the d-axis current. (6) is used to predict the dc-bus power for each and is represented by dotted, solid, and dashed curves.

#### A. MPPT Illustration

The simulation model in Fig. 9(a) is used to show how the proposed integrated generator-rectifier system can be employed to accomplish MPPT. The rotational speed  $\omega$  of a wind turbine with dynamics is used as the generator's reference speed.

$$J\omega \frac{d\omega}{dt} = P_{\text{turbine}} - P_{\text{dc}} \quad (11)$$

where  $J$  is the moment of inertia of the wind turbine, which has been set to  $28.7 \times 10^6 \text{ kg}\cdot\text{sq}\cdot\text{m}$ . This number was chosen to be 50 times lower than a realistic value for a 10 MW turbine [30] to save simulation run time. The turbine power  $P_{\text{turbine}}$  follows the mechanical power curve in Fig. 7 for each wind speed. The MPPT algorithm in Fig. 5 uses the turbine rotational speed as the feedback signal to set the power controller reference value to follow the maximum-power curve in Fig. 7

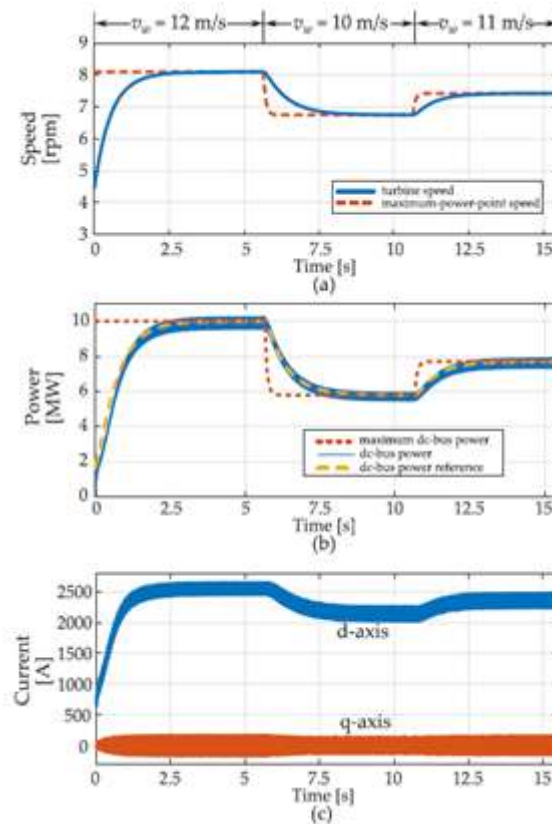
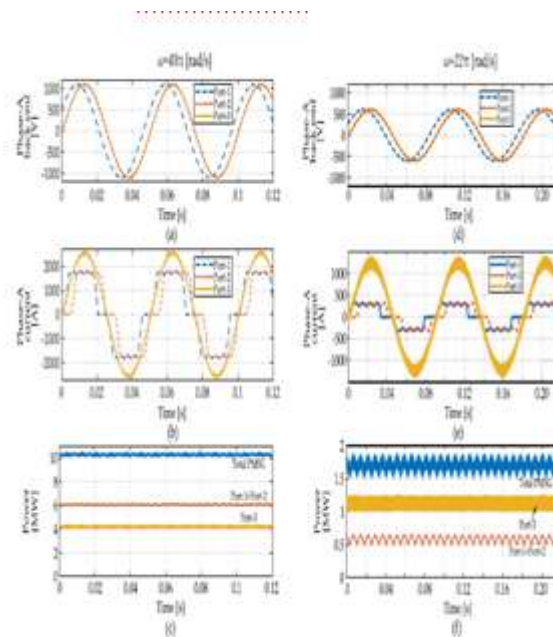


Fig. 10 shows that the proposed integrated generator-rectifier architecture tracks the wind-turbine maximum power point.

The turbine is spinning at 55% of its rated speed at time zero, and the wind speed is 12 m/s. The maximum power output of the turbine is 10 MW, while the dc bus is directed to draw 2 MW. The MPPT algorithm boosts the power command delivered to the power controller when the turbine speed increases [as shown by the solid-blue line in

Fig. 10(a)], as illustrated by the dotted-orange line in Fig. 10(a) (b) When the electrical output equals the maximum power, the wind turbine will settle to its optimal speed, and 10 MW will be taken. Figure 10 depicts the corresponding d-axis and q-axis currents (c).



This technique is also depicted in Fig. 10 at different wind speeds. The wind speed changes to 10 and 11 m/s at instances 5.5 and 10.5 s, respectively. The MPPT controller adjusts its power command in response to changes in windspeed, as indicated by the dashed yellow line in Fig. 10. (b). The reference power is tracked by the dc-bus power, allowing the turbine to revolve at the best speed for maximum power extraction.

### C. PMSG Torque Ripple and Power Quality Assessment

This section calculates the effects of distorted ac currents caused by diode-bridge operation on total PMSG power quality and calculates generator torque ripple.

At the 20-Hz rated electrical frequency, Fig. 11(a) illustrates the phase-A back EMFs

corresponding to Port-1, Port-2, and Port-3. The phase-A currents of the three ac ports are illustrated in Fig. 11 at 10-MW rated power drawn by the dc-bus (b). As expected, the currents corresponding to the diode bridges are nonsinusoidal.

As illustrated in Fig. 11, the total PMSG input power is computed by aggregating the instantaneous power output of all back EMF sources (c). To accommodate for generator resistive losses, the total input power is somewhat more than 10 MW. The passive rectifiers linked to Port-1 and

Port-2 process 60 percent of the total power. The ripple factor is used to quantify the input power ripple. It is defined as the ratio between the ripple-power rms value and the dc power value. The ripple factor is 0.4 percent in the rated condition.

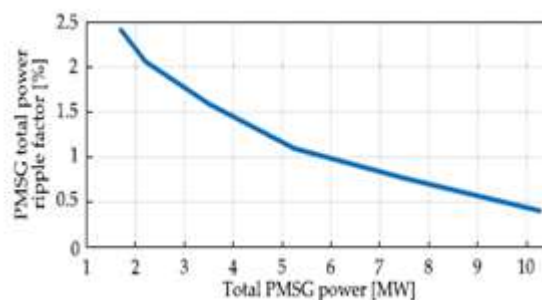


Fig. 12. Ripple factor of the total PMSG power is always below 2.5% and decreases as the output power increases.

After that, the ripple factor variation as a function of the generator speed is evaluated. Input

electricity from the generator the frequency and amplitude of the back EMF are related to the speed

of the generator. As a result, both decline. At a minimum operating speed of 55 percent of the specified speed as depicted in Figure 11 (d). The ac-port currents vary, as do the voltages. Figure 11(e) shows how to deliver the quantity of power shown. Figure 11 (f). The input power of a wind turbine is proportional to the generator speed cube [23], resulting in the At the minimum operating speed, the input power will be 1.7 MW. In contrast to Fig. 11(c), the majority of the electricity is processed by the processor. As shown in Fig. 11(f), an active rectifier is connected to Port-3. The ripple factor is 2.4%. Fig. 12 shows the ripple factor for the entire operating speed range as a function of the input power. The mechanical speed of a wind turbine can be considered relatively constant within the time scale of the electrical dynamics due to its large inertia. As a result, the torque ripple is the same as the power ripple. The ripple factor of the integrated generator–rectifier system is less than the permitted range of 5%–10% [31], [32].

### CONCLUSION

An MPPT methodology for an integrated generator–rectifier system is presented in this paper. A mathematical relationship is developed between the dc-bus power and the active-rectifier d-axis current. Both simulation and experiment were used to validate the model. A For practical implementation, a cascaded control architecture is proposed. The inner loop is made up of PI current controllers. The inner loop is a feed-forward loop, whereas the outer loop is a PI power controller. Power tracking performance that is satisfactory has been achieved. The wind turbine MPPT is enabled through power flow control. Controlling the dc-bus power is one way to do this. This talent opens up new possibilities. Integrated generator–rectifier systems have a lot of potential in the future.

Applications for wind energy

### REFERENCES

- [1]. P. Huynh, S. Tungare, and A. Banerjee, “Maximum power point tracking for wind turbine using integrated generator-rectifier systems,” in Proc. IEEE Energy Convers. Congr. Expo., Sep. 2019, pp. 13–20.
- [2]. D. S. Ottensen, “Global offshore wind market report,” Norwegian Energy Partner, Oslo, Norway, Tech. Rep. 02092019, 2018.
- [3]. C. Bak et al., “Light rotor: The 10-MW reference wind turbine,” in Proc. Eur. Wind Energy Conf. Exhib., 2012, pp. 1–10.
- [4]. P. Higgins and A. Foley, “The evolution of offshore wind power in the United Kingdom,” *Renewable Sustain. Energy Rev.*, vol. 37, pp. 599–612, 2014.
- [5]. W. Musial, P. Beiter, P. Spitsen, J. Nunemaker, and V. Gevorgian, “2018 offshore wind technologies market report,” National Renewable Energy Laboratory, Golden, CO, Canada, Tech. Rep., Aug. 9, 2019. [Online]. Available: <https://www.energy.gov/eere/wind/downloads/2018-offshorewind-market-report>
- [6]. Siemens Gamesa, “SG 10.0-193DD Offshore wind turbine,” Jan. 16, 2019. [Online]. Available: <https://www.siemensgamesa.com/en-int/productsand-services/offshore/wind-turbine-sg-10-0-193-dd>
- [7]. GE Renewable Energy, “Haliade-X 12 MW offshore wind turbine platform,” Sep. 19, 2019. [Online]. Available: <https://www.ge.com/renewableenergy/wind-energy/offshore-wind/haliade-x-offshore-turbine>
- [8]. MHI Vestas Offshore Wind, “The world’s most powerful available wind turbine gets major power boost,” Dec. 4, 2017. [Online]. Available: <http://www.mhivestasoffshore.com/worlds-most-powerful-available-wind-turbine-gets-major-power-boost/>
- [9]. V. Yaramasu, B. Wu, P. C. Sen, S. Kouro, and M. Narimani, “High-power wind energy conversion systems: State-of-the-art and emerging technologies,” *Proc. IEEE*, vol. 103, no. 5, pp. 740–788, May 2015.
- [10]. M. Chinchilla, S. Arnaltes, and J. C. Burgos, “Control of permanent magnet generators applied to variable-speed wind-energy systems connected to the grid,” *IEEE Trans. Energy Convers.*, vol. 21, no. 1, pp. 130–135, Mar. 2006.
- [11]. J. Lu, S. Golestan, M. Savaghebi, J. C. Vasquez, J. M. Guerrero, and A. Marzabal, “An enhanced state observer for dc-link voltage control of three-phase AC/DC converters,” *IEEE Trans. Power Electron.*, vol. 33, no. 2, pp. 936–942, Feb. 2018.